Supporting information

Experimental

1 Materials

Zinc acetate dihydrate ($C_4H_6O_4Zn{\cdot}2H_2O$), potassium hydroxide (KOH), anhydrous potassium carbonate (K_2CO_3), hydrochloric acid (HCl) and iron nitrate nonahydrate ($Fe(NO_3)_3{\cdot}9H_2O$) were purchased from Sinopharm Chemical Reagents Co., Ltd. 2-methylimidazole ($C_4H_6N_2$) was purchased from Shanghai Macklin Biochemical Technology Co., Ltd. Boric acid (H_3BO_3) was purchased from Hunan Huihong Reagent Co., Ltd. All reagents were used without further purification.

2 Preparation of ZIF-8

ZIF-8 was synthesized through a wet chemistry method. In detail, 7.2 g of $C_4H_6O_4Zn{\cdot}2H_2O$ and 30 g of $C_4H_6N_2$ were dissolved in 200 mL of deionized water by magnetic stirring at room temperature, respectively. The above two solutions were thoroughly mixed, and then aged for 48 h at room temperature. The obtained white precipitate was collected and washed three times by methanol and deionized water respectively, and dried at 60 °C for 8 h.

3 Carbonization of ZIF-8 (ZIF-8-800)

The ZIF-8 powder was transferred into a tube furnace and annealed at 800 °C for 1 h under argon with a heating rate of 5 °C/min. Subsequently, the obtained product was thoroughly washed with 35 wt% hydrochloric acid and deionized water, respectively, filtered and dried at 60 °C for 8 h.

4 Preparation of ZIF-8-derived porous carbons

ZIF-8-800 and activator (KOH, H_3BO_3 or $Fe(NO_3)_3$) were mixed in an appropriate amount of deionized water at a mass ratio of 1:2. Then, the mixed suspension was stirred at 80 °C to evaporate deionized water. The obtained powder was dried at 60 °C for 8 h. The dried powder was further transferred to a tube furnace and activated at 700 °C for 2 h under argon with a heating rate of 5 °C/min. The activated product was thoroughly washed with 35 wt% hydrochloric acid and deionized water, filtered and dried at 60 °C for 8 h. ZIF-8-800 activated with KOH, H_3BO_3, $Fe(NO_3)_3$ were labeled as ZIF-8-800(KOH), ZIF-8-800(H_3BO_3) and ZIF-8-800($Fe(NO_3)_3$), respectively.

5 Material characterization

Powder X-ray diffraction analysis was performed on an Bruker D8 Advance diffractometer with a Cu K_α radiation source. The morphology of the prepared powders was characterized by a JSM-7610Fplus scanning electron microscope equipped with an energy dispersion spectroscopy. Raman spectra were collected on an inVia Reflex spectrometer. The specific surface area and pore size of the prepared powder were measured by an ASAP2020 N2 adsorption-desorption instrument.

6 Electrochemical measurements

The electrochemical performance of ZIHCs using ZIF-8-derived porous carbon cathodes was investigated using 2023-type coin cells. In the assembly of ZIHCs, ZIF-8-800, ZIF-8-800(H_3BO_3), ZIF-8-800($Fe(NO_3)_3$) and ZIF-8-800(KOH) were used as cathodes to match commercial zinc foil anodes whose surface was first polished by the sandpaper to remove oxide layer before use. A glass fiber as a separator filled with zinc sulfate electrolyte is sandwiched

between the cathodes and anodes. The fabrication of cathode is by mixing active materials (ZIF-8-800, ZIF-8-800(H_3BO_3), ZIF-8-800($Fe(NO_3)_3$) and ZIF-8-800(KOH)), polyvinylidene fluoride binder and acetylene black conductive agent in 1-methyl-2-pyrrolidone solvent with at a mass ratio of 8:1:1 to form a uniform slurry. The slurry was coated on a stainless steel foil by a doctor blade and dried at 60 °C for 8 h. Mass loading of active materials is around 1 mg/cm^2. The thickness of the electrode is about 25 μm. Galvanostatic charge-discharge tests were performed on the CT-3008-5V10Ma-164 high-precision electrochemical performance test system at current densities of 0.1 and 1 A/g. Cyclic voltammetry (CV) tests were conducted at a scan rate from 5 to 50 mV/s. Electrochemical impedance spectroscopy (EIS) measurements were performed at a frequency ranging from 0.1 Hz to 1 MHz with an amplitude of 5 mV. CV and EIS were measured on an RST5000 electrochemical workstation. The specific capacitance, energy density and power density were calculated according to Eqs. (1)−(3) [1–3].

$$C = \frac{I\Delta t}{m\Delta V} \quad (1)$$

$$E = \frac{C(V_{max}^2 - V_{min}^2)}{2\times 3.6} \quad (2)$$

$$P = \frac{E\times 3600}{\Delta t} \quad (3)$$

where I, Δt, m and ΔV represent the charge and discharge current, the discharge time, the mass of the active material in the working electrode and the voltage window, respectively.

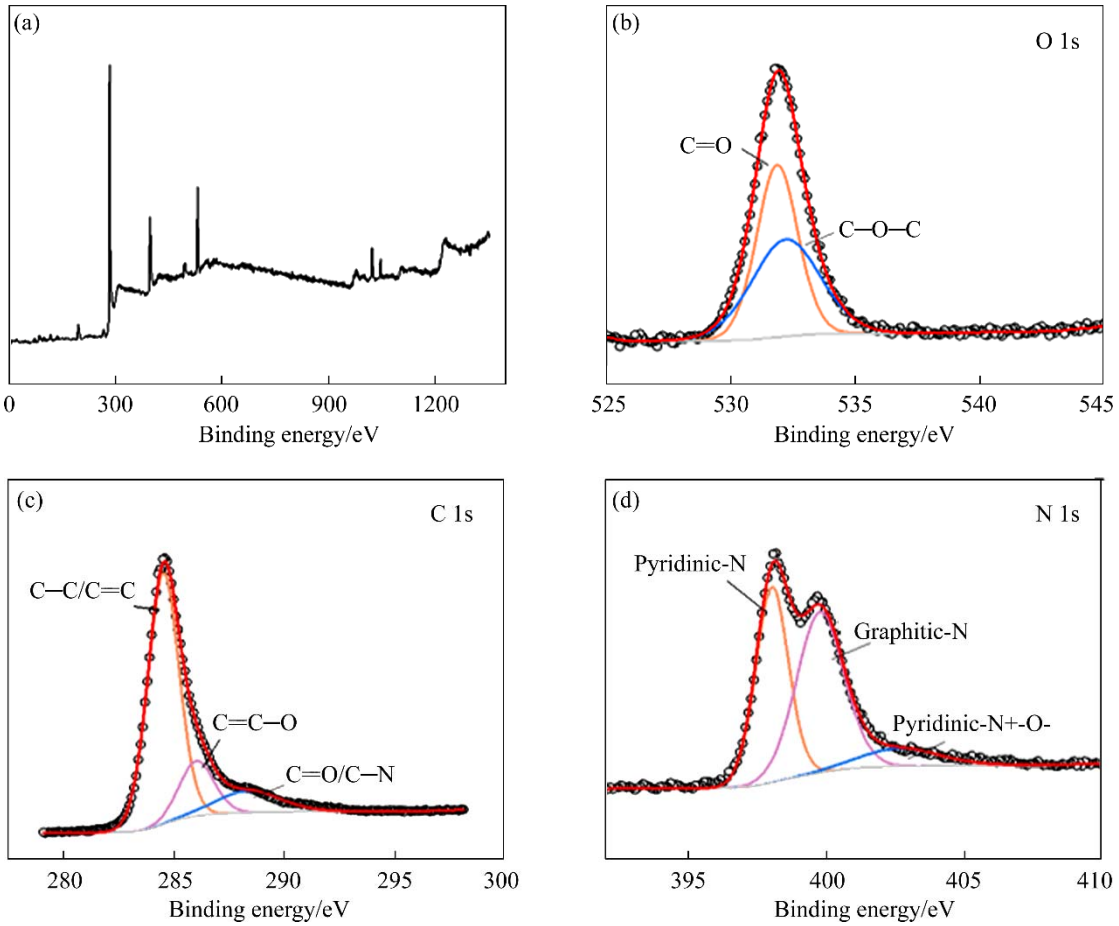

Figure S1 (a) XPS survey, high resolution (b) O 1s, (c) C 1s and (d) 1s spectra of ZIF-8-800

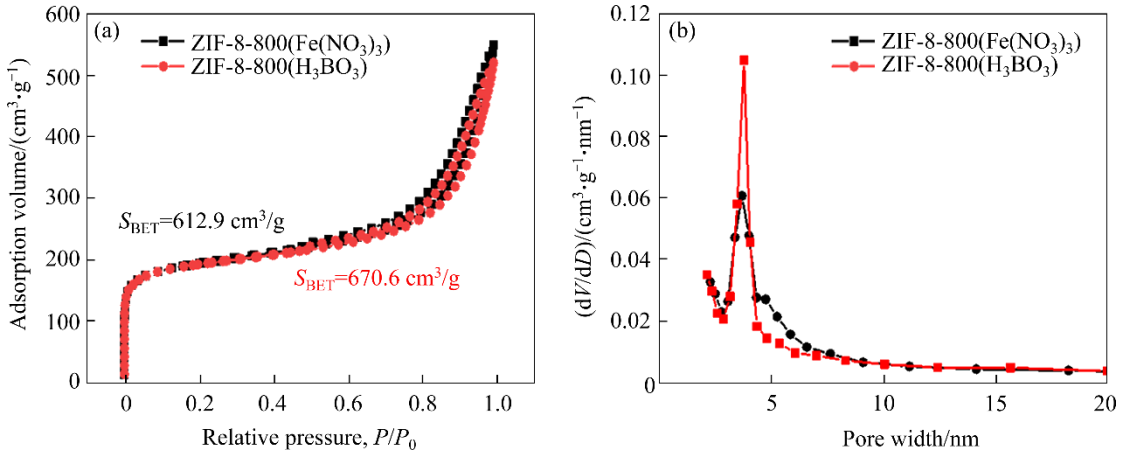

Figure S2 (a) The N2 adsorption/desorption isotherms and (b) the pore size distribution of ZIF-8-800($Fe(NO_3)_3$) and ZIF-8-800(H_3BO_3)

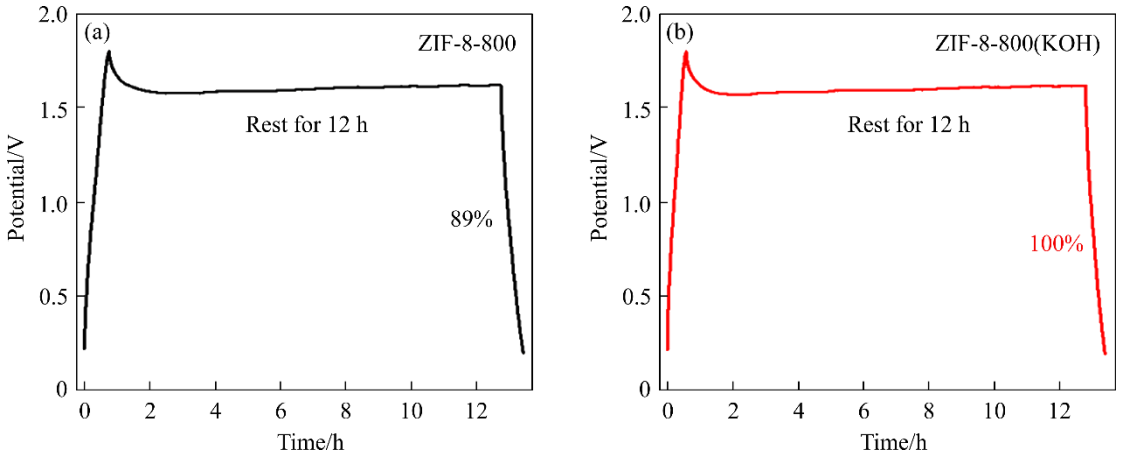

Figure S3 Charge and discharge curves of ZIHCs using (a) ZIF-8-800 and (b) ZIF-8-800(KOH) cathodes with a rest of 12 h

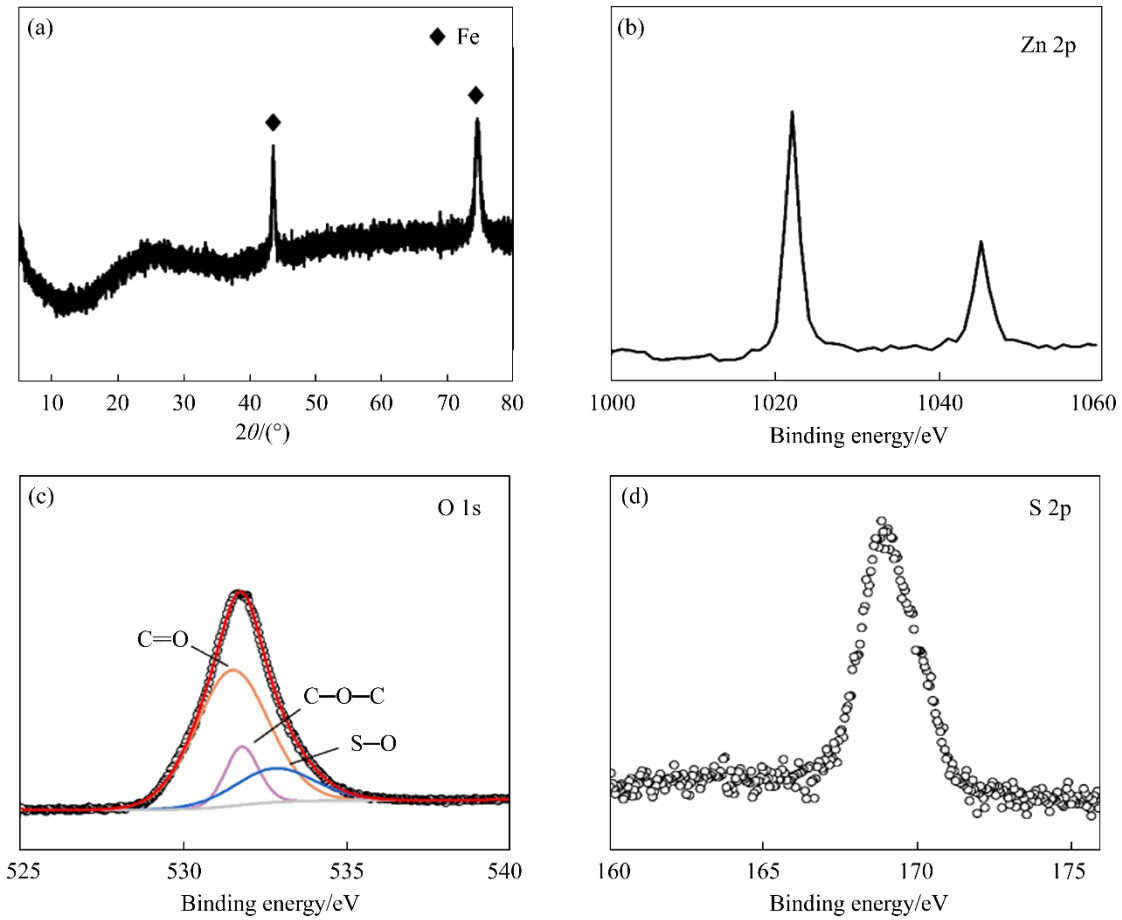

Figure S4 (a) XRD patterns and (b, c, d) XPS spectra of ZIF-8-800(KOH) cathode in ZIHCs after cycling

XRD patterns show no impurity peaks except for the iron phase of the stainless steel substrate. However, pronounced zinc, oxygen and sulfur signals are observed in the XPS spectra of the post-cycling electrodes. The Zn 2p at 1022 and 1045 eV and S 2p spectra at 168.9 eV can be indexed as Zn^{2+} and SO_4^{2-} ions, respectively. In addition, a new peak is formed in the binding energy of 532.7 eV of O 1s, which is assigned to the S—O bond. Based on this, the byproducts on the post-cycled electrode are supposed to be zinc hydroxide sulfate, which is consistent with previously reported byproducts on manganese and vanadium-based cathodes in aqueous zinc-ion batteries.

Table S1 Rate performance of ZIF-8-800(KOH) compared with previously reported porous carbon

Material	Electrolyte	Current density/($A \cdot g^{-1}$)	Capacitance/($F \cdot g^{-1}$)	Reference
ZIF-8-800(KOH)	$ZnSO_4$	0.10	375.5	This work
		1.00	203.0	
N, O-doped honeycomb-carbon	$ZnSO_4$	0.05	218.0	[4]
Potato derived porous carbon		0.50	336.0	[5]
Chitosan aerogel derived hierarchical porous carbon	$ZnSO_4$	2.00	165.6	[6]
Nitrogen and oxygen co-doped carbon	$Zn(CF_3SO_3)_2$/DMF	20.00	151.0	[7]
	$ZnSO_4$	20.00	181.2	
Cotton fabric derived hierarchically porous carbon	KOH	10.00	90.0	[8]
Nitrogen-doped tubular carbon	H_2SO_4-$ZnSO_4$	10.00	181.3	[9]

Table S2 Comparison of electrochemical properties of ZIF-8-800(KOH) with previously reported capacitors

Material	Electrolyte	Current density	Cycling number	Capacity retention/%	Ref.
ZIF-8-800(KOH)	$ZnSO_4$	0.1 A/g	100	89.20	This work
		1 A/g	9000	77.80	
PCN	$ZnSO_4$	1 A/g	4000	90.80	[10]
N, O, and S tri-doped hierarchical porous carbon	$ZnSO_4$	2 A/g	8000	88.00	[11]
ZnLFK-PC	$ZnSO_4$	10 A/g	4000	92.40	[12]
$NiCo_2O_4$//Fe_3Mo_3C/ Mo_2C@CNTs-800	KOH	1 A/g	4000	73.90	[13]
COCVO-2//AC ASC	KOH	30 mA/cm^2	5000	84.65	[14]
Ni-MOF@PANI-rGO	KOH	8 A/g	5000	90.00	[15]

References

[1] PECH D, BRUNET M, DUROU H, et al. Ultrahigh-power micrometre-sized supercapacitors based on onion-like carbon [J]. Nkature Nanotechnology, 2010, 5: 651−654. DOI: 10.1038/nnano.2010.162.

[2] GOGOTSI Y, SIMON P. True performance metrics in electrochemical energy storage [J]. Science, 2011, 334(6058): 917−918. DOI: 10.1126/science.1213003.

[3] MILLER J R, SIMON P. Electrochemical capacitors for energy management [J]. Science, 2008, 321(5889): 651−652. DOI: 10.1126/science.1158736.

[4] QIU Bao-ping, WEI Xiang, ZHANG Wei, et al. Shrimp shell-derived N, O-doped honeycomb-carbon for high-performance supercapacitor [J]. Diamond and Related Materials, 2023, 136: 110041. DOI: 10.1016/j.diamond.2023.110041.

[5] HU Hong-yu, WU Guo-jiang. Porous carbon derived from sweet potato biomass as electrode for zinc-ion hybrid supercapacitors [J]. International Journal of Electrochemical Science, 2021, 16(9): 210937. DOI: 10.20964/2021.09.01.

[6] ZHANG Yu, WANG Li-hua, JIA De-dong, et al. Hierarchical porous doped carbon plates derived from chitosan aerogel as cathode for high performance Zn-ion hybrid capacitor [J]. Chem Electro Chem, 2023, 10(4): e202200972. DOI: 10.1002/celc.202200972.

[7] ZHANG Yi, XIE Peng-cheng, JIANG Chun-hai, et al. Nitrogen and oxygen Co-doped carbon micro-foams derived from gelatin as high-performance cathode materials of Zn-ion capacitors [J]. Journal of Energy Storage, 2023, 57: 106169. DOI: 10.1016/j.est.2022.106169.

[8] CHEN Long, JI Tuo, MU Li-wen, et al. Cotton fabric derived hierarchically porous carbon and nitrogen doping for sustainable capacitor electrode [J]. Carbon, 2017, 111: 839−848. DOI: 10.1016/j.carbon.2016.10.054.

[9] YUKSEL R, BUYUKCAKIR O, PANDA P K, et al. Necklace-like nitrogen-doped tubular carbon 3D frameworks for electrochemical energy storage [J]. Advanced Functional Materials, 2020, 30(10): 1909725. DOI: 10.1002/adfm.201909725.

[10] ZHANG Ya-min, WANG Zhong-pu, LI De-ping, et al. Ultrathin carbon nanosheets for highly efficient capacitive K-ion and Zn-ion storage [J]. Journal of Materials Chemistry A, 2020, 8(43): 22874−22885. DOI: 10.1039/D0TA08577D.

[11] MA Jian-hui, YANG Shun-sheng, HUANG Tao, et al. 3D hierarchical tri-doped porous carbon derived from calcium lignosulfonate for high-performance zinc ion hybrid capacitors [J]. New Journal of Chemistry, 2023, 47(37): 17549−17557. DOI: 10.1039/D3NJ03537A.

[12] LIU He-yang, CHEN Han-sheng, SHI Kai-yuan, et al. Lignin-derived porous carbon for zinc-ion hybrid capacitor [J]. Industrial Crops and Products, 2022, 187: 115519. DOI: 10.1016/j.indcrop.2022.115519.

[13] HU Rui-yang, LIU Li-yuan, HE Jia-hao, et al. Preparation and electrochemical properties of bimetallic carbide Fe_3Mo_3C/Mo_2C@carbon nanotubes as negative electrode material for supercapacitor [J]. Journal of Energy Storage, 2023, 72: 108656. DOI: 10.1016/j.est.2023.108656.

[14] JIAO Zhi-chao, CHEN Yuan-qing, DU Miao, et al. In-situ formation of morphology-controlled cobalt vanadate on CoO urchin-like microspheres as asymmetric supercapacitor electrode [J]. Journal of Alloys and Compounds, 2023, 958: 170489. DOI: 10.1016/j.jallcom.2023.170489.

[15] AMIRABAD T N, ENSAFI A A, MOUSAABADI K Z, et al. Binder-free engineering design of Ni-MOF ultrathin sheet-like grown on PANI@GO decorated nickel foam as an electrode for in hydrogen evolution reaction and asymmetric supercapacitor [J]. International Journal of Hydrogen Energy, 2023, 48(76): 29471−29484. DOI: 10.1016/j.ijhydene.2023.04.159.